ACS SENSORS

pubs.acs.org/acssensors

Article

Microfluidic Biosensor for Rapid Nucleic Acid Quantitation Based on Hyperspectral Interferometric Amplicon-Complex Analysis

Rongxin Fu, Wenli Du, Xiangyu Jin, Ruliang Wang, Xue Lin, Ya Su, Han Yang, Xiaohui Shan, Wenqi Lv, Zhi Zheng,* and Guoliang Huang*

Cite This: *ACS Sens.* 2021, 6, 4057–4066

Read Online

ACCESS | Metrics & More | Article Recommendations | Supporting Information

ABSTRACT: Nucleic acid detection plays a vital role in both biomedical research and clinical medicine. The temperature circulation changes of the widely used polymerase chain reaction technique are time-consuming and technically challenging for system development. Recombinase polymerase amplification (RPA) is an isothermal method for rapid nucleic acid detection. However, current RPA amplicon detection methods are complicated and expensive and easily generate false positives, restricting the promotion of RPA techniques. In this work, a hyperspectral interferometric amplicon-complex quantitation method is presented, combined with asymmetric dipole complex strategy optical scattering analysis. GelRed dye was utilized to form amplicon-complex particles, and the Fourier domain spectrum computation contributed to complex scattering quantitation. With this method, a supporting microfluidic chip and automatic system were developed to achieve integrated, rapid, quantitative, and miniscule nucleic acid detection. The *Plasmodium falciparum dhfr* gene was utilized as an example for targeted nucleic acid quantitation and single nucleotide polymorphism detection. The total reaction time was decreased to merely 20 min, and the limit of detection was only 3.17 ng/μL. The minimum measurable concentration of target was 1.68 copies/μL, 31.67 times more sensitive than turbidity detection, and the single reaction chamber was only 9.33 μL. No scattering increase occurred for template-free control, and thus, false positives caused by primer dimers and nonspecific products could be avoided. The experimental results prove that the provided method and system can detect single-base mutations in the *dhfr* gene and is a reasonable technique for rapid, automatic, and low-cost nucleic acid detection.

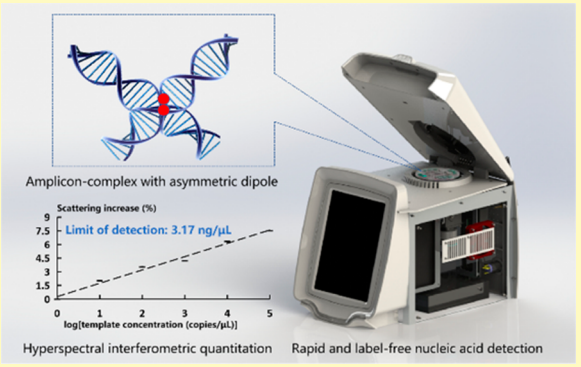

KEYWORDS: *microfluidic biosensor, recombinase polymerase amplification, hyperspectral interferometry, optical scattering analysis, malaria detection*

Downloaded via TSINGHUA UNIV on November 9, 2022 at 13:32:59 (UTC).
See https://pubs.acs.org/sharingguidelines for options on how to legitimately share published articles.

Nucleic acid detection is of vital importance in clinical diagnosis, disease treatment, drug discovery, during public health emergencies, and in other biomedical applications.[1−3] For instance, SARS-CoV-2 virus has caused >182 million infections and 4 million deaths since 2019 (up to Jul. 2021).[4] Targeted nucleic acid testing contributes to disease diagnosis, virus spread prevention, and drug treatment plan determination as well. Thus, rapid, low-cost, and easy-to-use nucleic acid detection methods and devices are extremely important.[5−7] Most current nucleic acid detection techniques utilize polymerase chain reaction (PCR) as the amplification approach, which is quite stable and quantitative.[8] However, the temperature circulation changes required by PCR are time-consuming and difficult to easily address for system development. Taking SARS-CoV-2 virus detection as an example, testing with PCR commonly requires >90 min, and multiple experimental processes are required with various pieces of scientific equipment.[9] In contrast, isothermal amplification methods can decrease the testing time by more than half. For instance, the multi-index isothermal amplification platform presented by Xing et al. yields results in 35 min.[10] Similarly, the time to results of the low-cost and scalable isothermal platform by Wang et al. is only 25 min,[11] and the ID now system of Abbott only requires 5 min to obtain results for high-concentration positive samples.[12] Thus, isothermal methods and devices have attracted tremendous interest in both academia and industry due to the obvious advantages in equipment convenience, personnel skill requirements, and detection time. Common isothermal amplification methods include loop-mediated isothermal amplification, rolling circle amplification, recombinase polymerase amplification (RPA),

Received: July 14, 2021
Accepted: October 11, 2021
Published: October 25, 2021

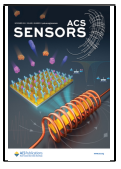

© 2021 American Chemical Society

https://doi.org/10.1021/acssensors.1c01491
ACS Sens. 2021, 6, 4057–4066

helicase-dependent amplification, and nuclear acid sequence-based amplification.[13−17] Especially, RPA owns the merits of high sensitivity, fast reaction speed, simple primer design, and independent of a strict experimental environment. Therefore, nucleic acid detection based on RPA has recently become a research hotspot.[18−20]

Unfortunately, there are still some problems to be solved with RPA techniques. RPA amplicon detection is the most difficult obstacle that restricts its popularization and application. Agarose gel electrophoresis detection requires multiple devices in combination and cannot be automated, making this method time-consuming and easily contaminated.[21] With re-purposing bridging flocculation, interference products such as primer dimers may cause a high risk of false positives.[22] Immunosorbent assays also lead to cross-contamination risks and make it difficult to avoid interference products without additional primers, causing high material costs.[23] Solid phase electrochemical or chemiluminescence methods require multiple incubation and cleaning processes,[24,25] steps which are always cumbersome and time-consuming. Surface-enhanced Raman scattering requires special optical instruments, and the characteristic peaks of the labeled amplicon need to be determined by experiments in advance.[26] Detection with SYBR Green I or other fluorescent dyes is affected by the recombinant enzyme, and thus, the accuracy is unsatisfactory.[27] Real-time fluorescent detection with RPA is similar to the TaqMan probe method of PCR, introducing an additional fluorescent probe. When the probe matches the amplicon sequence, a corresponding endonuclease or exonuclease will cut the probe, freeing the fluorophore and generating a fluorescent signal. However, the synthesis cost of these probes is much higher than that of common primers, greatly increasing the detection cost. Photo-bleaching also limits the stability of the signal, and fluorescent detection requires professional scientific instruments. This is especially true for the detection of low-volume samples where necessitating complex optical modulation and highly sensitive detection devices are needed.[28] The silicon-based resonator proposed by Shin et al. is a novel real-time RPA amplicon detection method. In this method, one of the RPA primers is chemically modified and fixed on a silicon-based substrate. During the reaction, amplicon products increase on the substrate, changing the resonance frequency and affecting the light intensity output. Such solid phase detection methods can effectively reduce the risk of nonspecific amplification of RPA, but the preparation of the silicon-based substrates is quite difficult and expensive.[29] In conclusion, low-cost and high-efficiency RPA amplicon detection will be needed to promote RPA technology, and this is an area requiring further study.

Recently, relevant work reported that double-stranded DNA (dsDNA) forms a dipole when inserted in an asymmetric bis intercalating dye, such as GelRed. The polarized dsDNA generates a nanoscale amplicon-complex under the London force, providing an opportunity for alternative RPA amplicon detection.[30] The amplicon complex in the reaction solution weakly scatters vertical incident light, implying the refractive index and mass content of the amplicon. Precise acquirement and accurate analysis of the weak scattering signal caused by the amplicon-complex mass is a potential approach to achieve efficient and low-cost RPA amplicon detection. This method directly measures the total content of the reaction products so that it does not rely on the approximate relation between the fluorescent intensity and amplicon content. Moreover, amplicon products do not need to be purified and recovered, so the detection can automatically be performed in the reaction chamber. However, the amplicon complex is nanoscale in size and can only be detected at high concentrations and in a large reaction volume. Thus, a state-of-the-art scattering analysis method is necessary and meaningful to provide an alternative way to solve these current problems.

In this work, a hyperspectral interferometric amplicon-complex quantitation method is presented. The coherent spectrum of the weakly scattered light is recorded and precisely analyzed to calculate the amplicon-complex mass content, achieving quantitative and isothermal nucleic acid detection with RPA. Furthermore, a microfluidic centrifugal chip is provided for small-volume and automatic target detection. In addition, a supporting system is presented, integrating nucleic acid amplification, amplicon detection, reaction condition supply, and hyperspectral interferometric analysis. With the presented method and system, the *Plasmodium falciparum dhfr* gene was utilized as an example for targeted nucleic acid detection quantitation and single nucleotide polymorphism (SNP) detection. Given that 150 million new malaria cases and two million deaths happen per year, *P. falciparum*, which is the most dangerous *Plasmodium*, is a quite meaningful detection target.[31] False positives caused by primer dimers and nonspecific products could be avoided. The experimental results proved that the presented method and system are reasonable for rapid, automatic, and low-cost nucleic acid detection.

METHODS AND MATERIALS

Chemicals and RPA Reactions. To prove the detection principle and performance, the *P. falciparum dhfr* gene was utilized as the detection target. A partial sequence of this gene was cloned into the pUC57 plasmid, and corresponding RPA primers were synthesized by Sangon Biotech (Shanghai, China). The detailed sequences of the target and primers are listed in the Supporting Information (Table S1). The plasmid was 10-fold serially diluted from 10^5 copies/μL to 10^1 copies/μL for later use. To demonstrate the SNP detection ability of the proposed method, four mutated *dhfr* genes and corresponding primers with single point mutations at the marked red base (aat, aat → att, aat → act, aat → agt) were synthesized by Sangon Biotech, and the detailed sequences are shown in the Supporting Information (Table S2).

RPA solution was constructed using a TwistAmp basic kit (TwistDx, England). For the off-chip experiments, 29.5 μL of rehydration buffer, 4.8 μL of primer mix (10 μM), and 8.2 μL of water were mixed, and 5 μL of the template was added. Then, the mixture was added to one dried enzyme pellet. Magnesium acetate (2.5 μL of a 280 mM solution) was added into the reaction mix to start the reaction. The mixture was shaken well and centrifuged before heating to 39 °C for 20 min. For the on-chip experiments, the mixture was proportionally reduced to 9.33 μL per detection chamber with the same reagents, proportions, and reaction time. Qubit fluorometric quantitation (ThermoFisher Scientific, USA) was used to determine the amplicon concentrations. The GelRed solution was purchased from Sigma-Aldrich, USA.

Hyperspectral Interferometric Detection. After amplification, when amplicon products are mixed with GelRed solution, dsDNA molecules are complexed by the bis intercalating dye. Because GelRed is asymmetric in its electrical property, the inserted dsDNA forms an asymmetric dipole and generates nanoscale amplicon complexes with electrostatic attraction. A large quantity of amplicon complexes can be treated as assemblies of nanoscale particles with diameters far less than the wavelength of visible light. According to first-order Born approximation theory, the effects caused by these particles on the illumination light can be ignored in solution due to the weak

https://doi.org/10.1021/acssensors.1c01491
ACS Sens. 2021, 6, 4057−4066

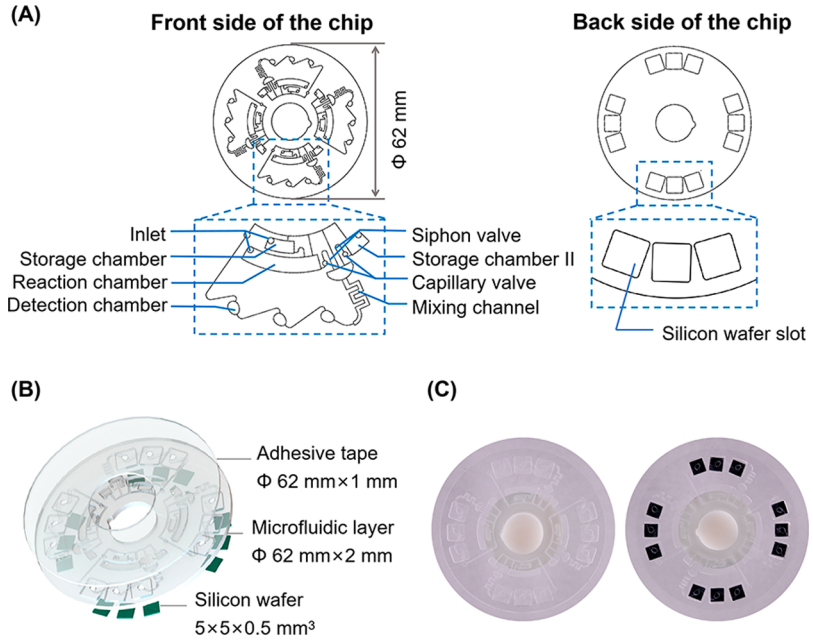

Figure 1. Design of the microfluidic chip. (A) Front and back sides of the chip with detailed chamber and valve descriptions. (B) Three layers and detailed size of the chip. (C) Photographs of the microfluidic chip with (right) and without (left) embedded wafers.

scattering property.[32] Then, the plane wave of the illumination light is defined as $U_0(k)$, where k donated the wavenumber, which equals the mean refractive index of the solution n_0 multiplied by the vacuum wavelength k_0. For the areas lacking amplicon complex, the illumination plane wave $U_0(k)$ is reflected twice at the wafer substrate. The one at the top surface of the monocrystalline silicon wafer is denoted as $U_1(k)$, and the other at the interface between the silicon layer and silica layer is denoted as $U_2(k)$. According to the wave propagation description, $U_1(k) = r_1U_0(k)e^{ikD}$ and $U_2(k) = r_2U_0(k)e^{ik(D+2d)}$, where D is the wave propagation distance in the solution and d is the thickness of the silica layer of the wafer substrate.[33] In this work, d = 900.15 nm, and this value was proved according to the previous publications.[34] r_1 and r_2 are the corresponding reflectance indices that can be calculated according to the Fresnel coefficient or thin film optical theory.[35] Assuming that when the plane wave $U_0(k)$ is scattered by a single amplicon-complex particle after propagating a distance of z ($z < D$), if the refractive index of the complex equals $n = \alpha n_0$, the scattering intensity can be calculated as $f(k) = (\alpha^2 - 1)k^2r^3\frac{\sin(qr) - qr\cos(qr)}{(qr)^3}$ according to the Rayleigh–Gans formula.[36] Herein, r is the radius of the single amplicon-complex nanoparticle, and q is the modulus of the scattering wave vector. Thus, the scattering signal of the amplicon-complex assemblies is $U_3(k) = \sum f(k)U_0(k)e^{ikz}$. Because the radius r is far less than the illumination wavelength, it can be approximated by $U_3(k) = \sum \frac{(\alpha^2 - 1)}{6}k_c^2r^3U_0(k)e^{ikz}$ because $\lim_{qr\to 0}\frac{\sin(qr) - qr\cos(qr)}{(qr)^3} = \frac{1}{6}$, where k_c is the average wavenumber in the solution.

With the above descriptions, for the areas lacking amplicon, the reflectance spectrum can be expressed as[37]

$$R_0(k) = \frac{|U_1(k) + U_2(k)|^2}{|U_0(k)|^2} = r_1^2 + r_2^2 + 2r_1r_2\cos(2kd) \quad (1)$$

where the amplicon complexes exist, the reflectance index can be expressed as $\frac{|[U_1(k) + U_2(k)]e^{ik(D-z)} + U_3(k)|^2}{|U_0(k)|^2}$. Considering that the scattering of particles will cause attenuation of reflectance beams, the reflectance spectrum can be expressed as

$$R_1(k) = \beta(k)R_0(k) + \sum_z R'(z)\cos[2k(D + d - z)] \quad (2)$$

here, $R'(z) = \frac{r_2(\alpha^2 - 1)}{3}m(z)k_c^2r^3$, $m(z)$is the number of amplicon-complex particles at the axial plane z, and $\beta(k)$ is the scattering attenuation coefficient due to particle scattering. It should be noted that the high-order terms of the scattering light, the interference items between the scattering light, and $U_1(k)$ are ignored because these items are far less than the remaining ones.

To quantitate the content of the amplicon-complex mass, the collected interferometric reflectance spectrum should be operated with fast Fourier transformation (FFT) along to the wavelength k. Then, a sequence of amplitude can be obtained, which is denoted as $R'(z)$. We define the total scattering increase as $S = \sum_{z>d}|R'(z) - R_0(z)|/\sum_{z>d}|R_0(z)| \times 100\%$, where $R_0(z)$ is the FFT amplitude result of the collected spectrum before RPA amplification. Based on the above calculation, S is a reasonable measurement of amplicon content. Please note that the above mathematical model exploits a necessary hypothesis: S can be treated as reliable estimation of amplicon-complex quantitation only if the radius of a single dsDNA-GelRed complex particle is nanoscale and meets the requirements of first-order Born approximation.

Microfluidic Chip. The proposed microfluidic chip is demonstrated in Figure 1, where Figure 1A shows the front and back sides of the chip. In general, the chip resembles a circular saucer with a central hollow section to affix it to the supporting system. On the front side, there are four repetitive units so that four various targets can be simultaneously detected. Each unit contains two storage chambers and a reaction chamber. Storage chamber I is used to store 6.2 μL of magnesium acetate solution, while storage chamber II is used to store 8 μL of 4000× GelRed solution. Each detection chamber is only 9.33 μL in volume. The width of the mix channel is 0.6 mm, and the depth is also 0.6 mm. The widths of the outlet channel of the reaction chamber and storage chamber I are 0.5 mm, and the depths are 0.5 mm. The width of storage chamber II is 0.6 mm, and the depth is 0.2 mm. On the back side of the chip, 12 5 mm × 5 mm wafers with a thickness of 0.5 mm are adhered with an ultraviolet glue. Figure 1B shows the three layers of the chip, which has a diameter of 62 mm. A 1 mm thick cover layer is adhered to the chip with an adhesive tape, and the chip is machined with polymethyl methacrylate (PMMA). The thickness of the PMMA layer is 2 mm. Figure 1C shows a photograph of the chip with no wafers on the left for display convenience and a wafer-containing version on the right.

https://doi.org/10.1021/acssensors.1c01491
ACS Sens. 2021, 6, 4057−4066

Before the experiments, the rehydration buffer, primer mix, and enzyme pellet (total volume = 13.8 μL) are added into the reaction chamber. When testing begins, the template solution is added to the reaction chamber through the inlet. Then, centrifugation at 1500 rpm with an acceleration of 2000 rpm/s is performed for 5 s to deposit the solution in storage chamber I into the reaction chamber. At the same time, the two capillary valves are run over, the liquid passes into the two siphon valves with the same liquid level as in the reaction chamber and storage chamber II. Next, centrifugation at 2000 rpm and an acceleration of 2000 rpm/s are performed for 5 s to force the residual liquid in storage chamber I into the reaction chamber. Next, a total of four centrifugation steps are utilized to completely mix the solution in the reaction chamber. First, the chip is centrifuged at 1000 rpm and 2000 rpm/s acceleration, followed by a speed of 2000 rpm and acceleration of 2000 rpm/s. Each centrifugal step occurs for 2 s, and thus, the entire mixing process lasts for 16 s. After mixing, the motor is stopped with an acceleration of 800 rpm/s, and then the liquid in the siphon valve passes through the siphon channels. At this time, heating begins to supply the temperature condition for RPA at 39 °C. After amplification, another centrifugal operation at 1000 rpm and 800 rpm/s acceleration is performed for 2 s to completely mix the solution in reaction chamber with the GelRed solution. The mixing channel is tortuous in shape to mix the liquid well and then push the solution into the three repetitive detection chambers.

Integrated Instrument. Figure 2 shows the electromechanical structure, optical design, and physical photograph of the system. In

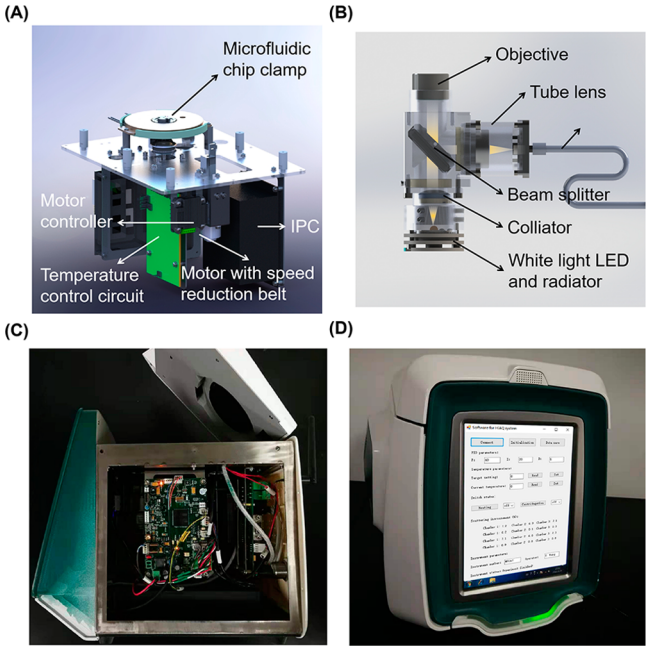

Figure 2. Design and photograph of the integrated system. (A) Electromechanical structure of the system. (B) Optical collection model design. (C) Photograph of the inner control circuits. (D) Photograph of the overall system with the GUI software.

Figure 2A, the chip clamp is used to fix the microfluidic chip, and the stepper motor (Z6000, Haydon, USA) with a speed reduction belt is used to provide a centrifugal rotation for the chip and position the detection chambers one by one at the optical focus for interference spectra acquisitions. The system is equipped with a motor control and temperature control module. An industrial personal computer (IPC, DX-1100, Dechengzhixing, China) is utilized for data storage, processing, and the graphical user interface (GUI). Figure 2B shows the design of the optical acquisition module. The beams of a whole-spectrum white LED (Bree Optronics, Jiangsu, China) with a homemade radiator pass through the collimator (#63-712, Edmund Optics, USA) and then a beam splitter (EBS1, Thorlabs, USA). The objective lens (10× Obj, CapitalBio, China) focuses 50% of the light onto the surface of the silicon wafer. The reflected light converges onto the optical fiber (M45L01, Thorlabs, USA) by the tube lens (#49-940, Edmund Optics, USA), and then a spectrometer (Maya2000, Ocean Optics, USA) connected to the IPC helps to collect the reflectance spectrum. Figure 2C shows the internal circuits of the system, and Figure 2d shows an overall image of the system including the control software.

RESULTS

Detection Principle Validation. Figure 3 shows microscopic images of dsDNA-GelRed complexes with different matter concentrations and the corresponding statistical results. The 4× and 10× micrographs were both recorded with the size of 1360 × 1024 pixels. Then, all of the images were binarized with a threshold of 183 using ImageJ software. The 4× microscopic images of 90 ng/μL dsDNA mixed with GelRed solution at different concentrations are listed in Figure 3A. The GelRed concentrations ranged from 500× to 8000× with two-fold steps. Moreover, Figure 3A shows the binarized image of the 2000× GelRed solution, as well as an example. The remaining pixel numbers were used as rough quantitation estimations of dsDNA-GelRed complexes. The statistical results of five independent experiments are shown in Figure 3B. For 4× microscopic images, from 500× to 8000× GelRed, the corresponding remaining pixel numbers were 5502 ± 110, 30 964 ± 734, 42 100 ± 2438, 64 358 ± 3567, and 63 775 ± 3376. For the 10× microscopic images, from 5000× to 8000× GelRed, the corresponding remaining pixel numbers were 6978 ± 223, 28 247 ± 566, 51 964 ± 3467, 82 068 ± 3689, and 80 292 ± 4782. We concluded that regardless of the magnification, the most reasonable GelRed concentration was 4000×. With this concentration, dsDNA molecules were completely transferred into dsDNA-GelRed complexes.

Similarly, 4× microscopic images of 4000× GelRed mixed with different dsDNA concentrations are shown in Figure 3C. The dsDNA concentration ranged from 0 to 100 ng/μL, with 20 ng/μL increases. The statistical results of five independent experiments are shown in Figure 3D. For the 4× microscopic images, from 0 to 100 ng/μL dsDNA, the corresponding remaining pixel numbers were 0 ± 0, 0 ± 0, 11 857 ± 391, 38 764 ± 1453, 846 321 ± 1763, and 78 634 ± 2354. For the 10× microscopic images, from 0 to 100 ng/μL dsDNA, the corresponding remaining pixel numbers were 0 ± 0, 0 ± 0, 16 999 ± 668, 33 451 ± 1521, 51 842 ± 1599, and 88 261 ± 6387. When the dsDNA concentrations were <40 ng/μL, microscopic images could not be used to detect the complex because no pixels remained after the binarization operation. Therefore, with this method, the minimum measurable concentration (MMC) of dsDNA occurred at 40 ng/μL. According to these results, dsDNA molecules could generate complexes when mixed with GelRed solutions, and when the concentration of the complexes was high enough, the complex assemblies could be detected by optical microscopy. However, when the concentration of the complexes was low, such as at dsDNA concentration <40 ng/μL, complexes would not form assembly masses and could not be measured due to the optical diffraction limit.

Microbeads Phantom and dsDNA-GelRed Complex Quantitation. To assess the quantitation performance of hyperspectral interferometric analysis for the weak scattering particles, 25 g/L polystyrene (PS) pellet solutions were diluted 4-, 8-, 16-, 32-, and 64-fold. All of these experiments were

https://doi.org/10.1021/acssensors.1c01491
ACS Sens. 2021, 6, 4057−4066

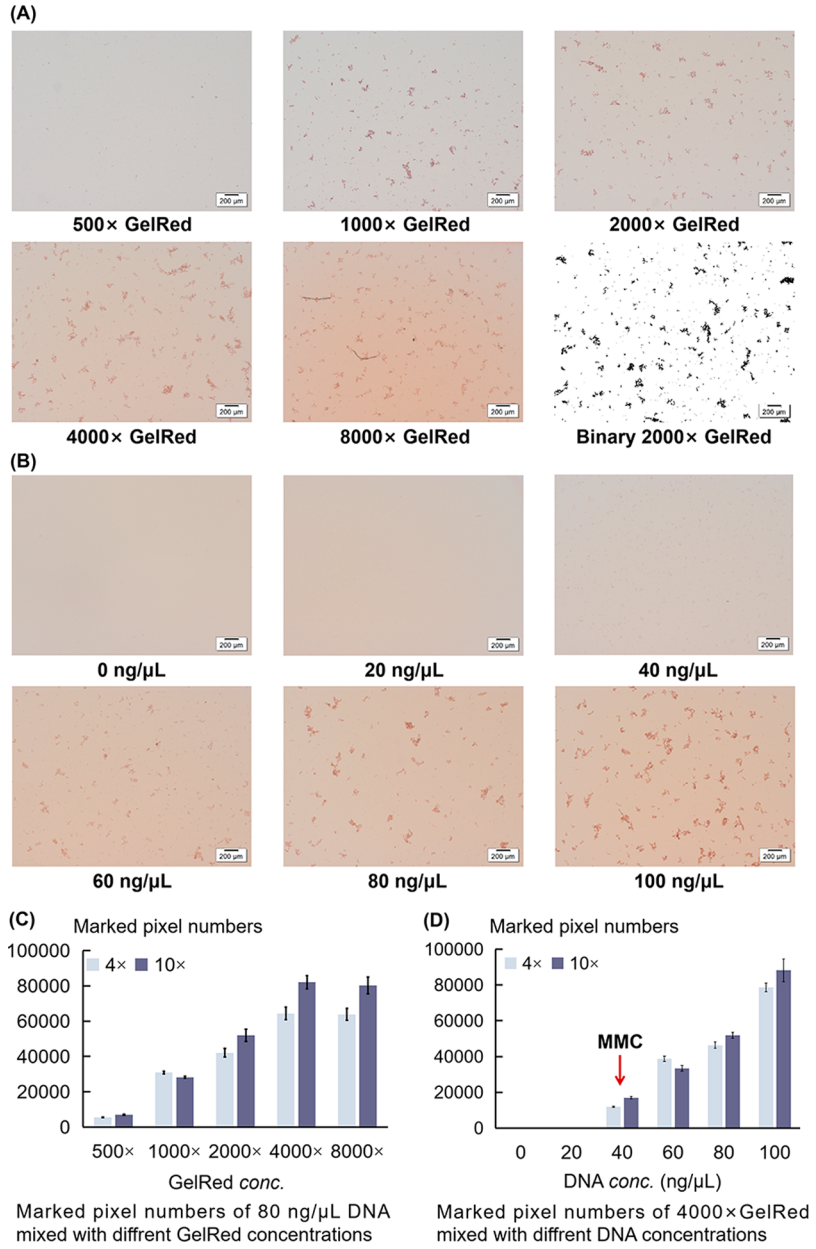

Figure 3. Validation of amplicon-complex generation and microscopic image statistics. (A) Microscopic images of 90 ng/μL dsDNA mixed with GelRed solutions at different concentrations. (B) Microscopic images of 4000× GelRed mixed with dsDNA at different concentrations. (C) Statistical results of panel A. (D) Statistical results of panel D. (MMC: minimum measurable concentration).

repeated five times. The corresponding scattering increases were 7.36 ± 0.21, 3.50 ± 0.18, 1.89 ± 0.14, 0.78 ± 0.00, and 0.71 ± 0.00%. The scattering increase of double-distilled H_2O was also measured, and the result was 0 ± 0.02%. Thus, taking the PS pellet concentration as x and the scattering increase as y, it could be acquired that $y = 1.161x + 0.0319$ ($R^2 = 0.9971$) using linear fitting. The interferometric spectra and statistical results are shown in Figure 4A,B. Similarly, synthetic dsDNA solutions were measured with concentrations of 0, 7.6, 15.9, 31, 62.2, and 126.5 ng/μL. All of the dsDNA samples were mixed well with 4000× GelRed solution. The corresponding scattering increases were 0 ± 0.06, 0.57 ± 0.02, 0.98 ± 0.07, 2.67 ± 0.01, 5.29 ± 0.06, and 11.22 ± 0.10%. Taking the dsDNA concentration as x and the scattering increase as y, it could be acquired that $y = 0.0895x - 0.1736$ ($R^2 = 0.9986$) using linear fitting.

According to these results, hyperspectral interferometry could quantitate PS and pure dsDNA samples with $R^2 > 0.99$, proving that the presented method meets the prerequisites for amplicon-complex quantitation. For dsDNA samples, the maximum standard deviation was 0.10%. The interferometric spectra and statistical results are shown in Figure 4C,D. To determine the limit of detection (LOD), three times the standard deviation divided by the fitting slope was calculated.[38] Therefore, the LOD for pure dsDNA samples was 3 × 0.10/0.0895 = 3.35 ng/μL.

Microfluidic Liquid Manipulation Process. Figure 5 shows the workflow of the microfluidic chip with three main steps. In Figure 5A, the reagents were added into storage chamber I, storage chamber II, and the reaction chamber. Figure 5B shows the designed condition for the amplification process. After the centrifugal operations, reagents in storage

https://doi.org/10.1021/acssensors.1c01491
ACS Sens. 2021, 6, 4057−4066

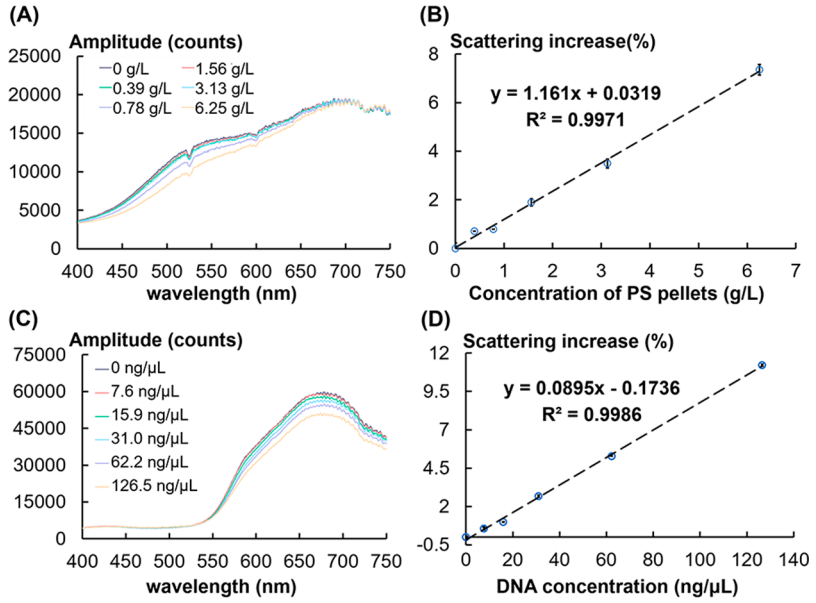

Figure 4. Interferometric spectra and scattering increase of PS pellets and dsDNA solutions at different concentrations. (A) Interferometric spectra of PS pellets at different concentrations. (B) Scattering increase of PS pellets at different concentrations. (C) Interferometric spectra of dsDNA at different concentrations. (D) Scattering increase of dsDNA at different concentrations. (Blue triangle for data points and black line for error bars).

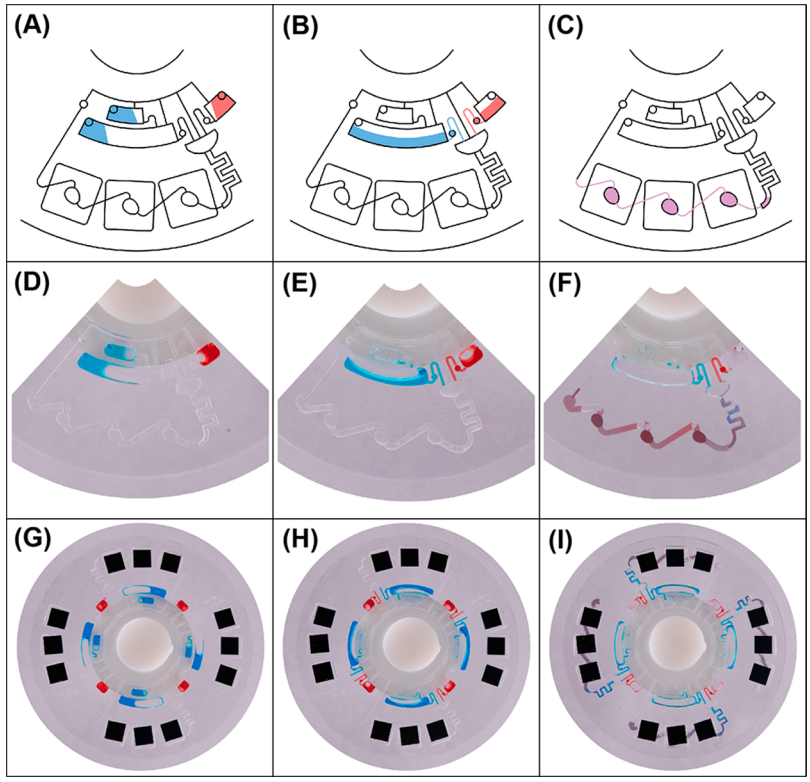

Figure 5. Step-by-step sketch of the microfluidic chip and corresponding experimental results. (A−C) Sketch of the three main steps. (D−F) Detailed corresponding results of the three steps. (G−I) Photographs of the entire chip during the three steps.

chamber I were totally transferred into the reaction chamber and mixed well. The liquid passed through the capillary valves and siphon valves and then flowed into the inlet of the mixing channel. The ratio of the depth of the left siphon valve to the right one was 5:2. With this ratio, the liquid in the two chambers would arrive at the inlet at the same time. At this moment, the supporting system began to heat the chip, and the RPA process started. Figure 5C shows the detection stage, where solution with amplicon was mixed with 4000× GelRed using the tortuous mixing channel and then transferred into the three repetitive detection chambers. Then, the motor rotated the chip to position the detection chambers, one by one, to the optical focus, and hyperspectral signals could be acquired.

Figure 5D−F shows photographs of a single unit during the three steps. For ease of visualization, the wafers were not

https://doi.org/10.1021/acssensors.1c01491
ACS Sens. 2021, 6, 4057−4066

placed in these sub-figures, and a blue ink was added to the amplification buffer. In Figure 5E, liquid in the reaction chamber and storage chamber II both passed through the valves and arrived at the inlet of the mixing channel. In Figure 5F, the mixing channel succeeded in efficient blending, yielding a uniform color distribution in the detection chambers without stratification. Figure 5G–I shows photographs of the whole chip with four units, demonstrating its repeatability.

RPA with Hyperspectral Interferometric Quantitation. To test the amplicon quantitative performance, off-chip RPA experiments were performed with template concentrations of 0, 10^1, 10^2, 10^3, 10^4, and 10^5 copies/μL. All of these experiments were repeated five times and the results are shown in Figure 6. Qubit was used to measure the average dsDNA concentrations, and the results were 0.24, 18.40, 26.00, 36.80, 58.00, and 70.60 ng/μL, respectively. Next, the solutions were added into the reaction chamber of the chip, and hyperspectral interferometric quantitation of the amplicons was conducted. The corresponding acquired scattering increases were 0 ± 0.10, 1.97 ± 0.04, 3.29 ± 0.07, 4.27 ± 0.04, 6.14 ± 0.11, and 7.42% ± 0.06%. Taking the amplicon concentration as x and scattering increase as y, it could be acquired that $y = 0.1042x + 0.1994$ ($R^2 = 0.9918$) using linear fitting. Because the samples were amplicon solutions with enzyme, ions, and other interference factors, compared with the results of pure DNA solutions, the fitting parameters changed and slightly decreased. Subsequently, the template samples with the introduced concentrations were utilized for absolute on-chip experiments. Similarly, these experiments were repeated five times. The corresponding acquired scattering increases were 0 ± 0.11, 2.01 ± 0.05, 3.52 ± 0.05, 4.21 ± 0.02, 6.33 ± 0.10, and 7.51 ± 0.07%. Taking the logarithm of template concentration as x and scattering increase as y, it could be acquired that $y = 1.4634x + 0.2734$, using linear fitting. Because the amplification reaction was not strictly linear, R^2 decreased to 0.9867, and the maximum standard deviation increased to 0.11%.

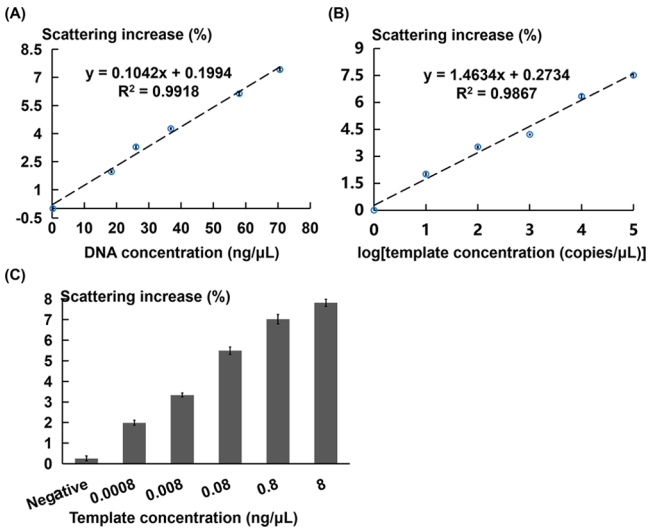

Figure 6. Hyperspectral interferometric quantitation of amplicons (A), templates (B), and real clinical samples (C) at different concentrations.

For amplicon solutions with inferring factors, the maximum standard deviation was 0.11% and the slope was 0.1042, yielding a LOD for amplicon samples of 3 × 0.11/0.1042 = 3.17 ng/μL. The values are nearly the same as that in pure DNA solutions, but the fitting parameters are slightly different. For the *dhfr* plasmid templates, the maximum standard deviation was 0.11% and the slope was 1.4634. Thus, the LOD was $10^{3\times0.11\div1.4634}$ = 1.68 copies/μL.

Moreover, to prove the performance of this work in practical applications, experiments with real sample experiments were conducted as well. In-vitro cultured *P. falciparum* samples, which had been collected from clinical malaria patients, were utilized as positive experimental targets with five different concentrations. Whole genome samples of human blood were used as the control group. All the in-vitro culture and lysis processes were conducted according to the previous publications.[39] The *P. falciparum* samples were lysed and diluted with the total DNA concentrations of 8.0, 8.0 × 10^{-1}, 8.0 × 10^{-2}, 8.0 × 10^{-3} and 8.0 × 10^{-4} ng/μL. All these experiments were repeated five times. As Figure 6C shows, the corresponding scattering increases were 7.81 ± 0.23, 7.02 ± 0.18, 5.49 ± 0.10, 3.34 ± 0.12 and 1.99 ± 0.12%. For the negative control, the scattering increase was 0.26 ± 0.17%. All experiment results of positive groups were 7.65 times larger than the control group so real *P. falciparum* detection could be achieved with the proposed biosensor and system.

SNP Detection. To prove the practical SNP detection ability of the presented biosensor, the *P. falciparum dhfr* gene was used as the target. SNPs in *P. falciparum dhfr* are related to drug resistance against *chloroquine*, *aminopyrimidine*, and other common malaria treatment drugs.[40] In the following experiments, all of the template samples were synthetic plasmids at a concentration of 10^6 copies/μL, and all experiments were repeated five times. Aside from the wild type *dhfr* gene sequence *dhfr-a* (aat), three mutant plasmids were also synthetized as *dhfr-t* (aat → att), *dhfr-a* (aat → act), and *dhfr-a* (aat → agt). Four forward primers (p-A, p-T, p-C, and p-G) were used with the same backward primer to amplify the four corresponding templates, and then scattering increases were detected with the proposed method and system. The detection results are shown in Figure 7. The electrophoresis results are displayed in Figure S1 in the Supporting Information.

For the *dhfr-a* template samples, using the four primer combinations in the order of atcg, the corresponding scattering increases were 9.07 ± 0.08, 6.18 ± 0.10, 6.49 ± 0.11, and 6.04 ± 0.10%. For *dhfr-t* template samples, using the four primer combinations in the same order, the corresponding scattering increases were 6.75 ± 0.02, 9.00 ± 0.13, 7.22 ± 0.10, and 6.61 ± 0.09%. For *dhfr-c* template samples with the same combinations in the same order, the corresponding scattering increases were 5.85 ± 0.02, 6.18 ± 0.10, 9.06 ± 0.15, and 6.00 ± 0.10%. For the *dhfr-g* template samples and the same primer combination order, the corresponding scattering increases were 5.22 ± 0.02, 5.42 ± 0.09, 4.99 ± 0.08, and 9.15 ± 0.15%. The maximum scattering increases happened at perfectly matched primers in every group. The maximum scattering increases were all ≥9.00% while the scattering increases were all <7.30% for the other experiments. The maximum standard deviation was only 0.15%. The SNP detection results proved that the presented biosensor could specifically recognize single-base gene mutations in *dhfr* for practical use.

https://doi.org/10.1021/acssensors.1c01491
ACS Sens. 2021, 6, 4057–4066

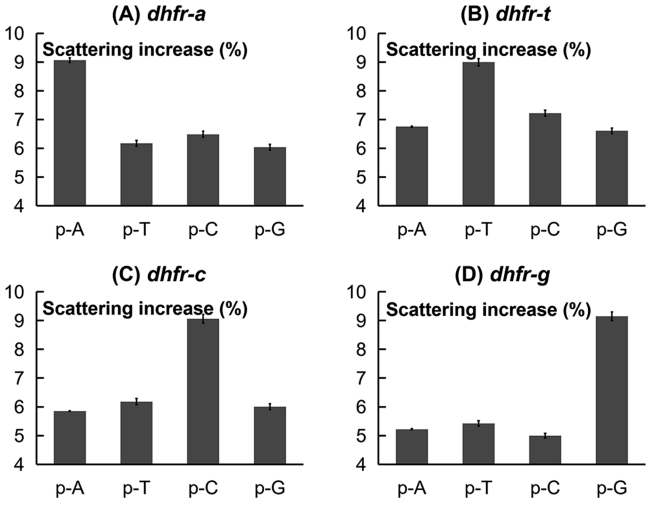

Figure 7. SNP detection results for the *dhfr* gene with four different genotypes. (A) Scattering increase of the *dhfr-a* gene with four amplification primers. (B) Scattering increase of the *dhfr-t* gene with four amplification primers. (C) Scattering increase of the *dhfr-c* gene with four amplification primers. (D) Scattering increase of the *dhfr-g* gene with four amplification primers. p-A, p-T, p-C, and p-G represented are the forward primers specifically designed to target each mutant.

DISCUSSION

In this paper, we presented three concepts as hyperspectral interferometric analysis, microfluidic chip, and the instrument. The key novelty is the hyperspectral interferometric method to analyze the optical amplicon-complex scattering and quantitate RPA products. The microfluidic chip and the instrument are both reasonable engineering choices to make the hyperspectral interferometric method achievable. The microfluidic chip was used to mix the amplicon and GelRed dyes, transfer liquid, and conduct RPA with microscale independent chambers. The instrument contributed to temperature control, chip movement, spectrum collection and analysis. With these two components, hyperspectral interferometric analysis can be carried out automatically and compactly, so the systematicness and integrity of this work can be presented. The instrument was modified with our previous work.[41] We re-designed the temperature control, spectrum collection, and control system including the GUI.

To compare the LOD with the traditional turbidity method, standard turbidity detection tests were performed with the samples in Figure 6B.[34] The results are displayed in Figure S2 in the Supporting Information. The maximum standard deviation was 0.32, and the slope was 0.5562. Therefore, the LOD for *dhfr* with turbidity detection was $10^{3\times0.3222\div0.5562}$ = 53.21 copies/μL, which is 31.67 worse than the presented biosensor. Compared with fluorescent RPA, the proposed method does not need additional exo-probe, which is approximately 150 times more expensive than ordinary probes. Furthermore, complicated fluorescence excitation and optical detection setup are no longer necessary. Fluorescent PCR and LAMP experiments were as well carried out for comparison. The detailed results and calculations were shown in Figure S3 in the Supporting Information. Briefly, with PCR, the LOD was 3.56 copies/μL, R^2 = 0.9916 and the detection time was 50 min (50 circles). With LAMP, the LOD was 2.92 × 10^5 copies/μL, R^2 = 0.9254 and the detection time was also 50 min. LOD of LAMP showed terrible performance due to the large C_T standard deviations for low template concentrations. With the presented method, the LOD was 1.68 copies/μL, R^2 = 0.9867 and the detection time was merely 20 min. It is obvious that the proposed method owns nearly equal LOD and fitting linearity as PCR but is much more rapid. Compared with LAMP, this work performed better in LOD, fitting linearity and time consuming.

The LOD performance of the biosensor is far better than microscopic image analysis and the traditional turbidity method. The first reason is that reflectance signals and scattering signals are segregated using Fourier transform. Because the scatter caused by amplicon complexes is quite weak, usually less than one-10th of the reflectance beam of the wafer, the Fourier transform helps to extract the scattering beams and increases the sensitivity. The second reason, which is more important, is that using microscopic image analysis and the traditional turbidity method, only the amplitude of the scattering beams can be recorded. The amplitude is $U_3(k)^2$ and proportional to the sixth order of the radius of a single scattering particle. Nevertheless, the coherent phenomenon of the reflectance beam and the scattering beam generates another multiplied item as $2U_1(k)U_3(k)$. This item is proportional to the third order of the radius of a single scattering particle. Given that the dsDNA and GelRed molecules are both much smaller than the wavelengths of visible light, the radius can be treated as close to zero. Without the three order attenuation, coherent items greatly enlarge the scattering signal. Meanwhile, because the amplitude of $U_1(k)$ is ten times larger than that of $U_3(k)$, the coefficient of the coherent item enlarges the scattering signal further. With the two strategies, the LOD value of our biosensor increased by 32.90-fold compared to traditional methods.

CONCLUSIONS

In this work, a microfluidic biosensor is presented for rapid nucleic acid detection based on hyperspectral interferometric amplicon-complex quantitation. Combined with quantitative interferometric scattering analysis and an amplicon-complex strategy, targeted nucleic acid could be detected in 20 min using the presented microfluidic chip and integrated instrument. RPA products could be quantitated with a LOD of 3.17 ng/μL using a reaction volume of 9.33 μL, and the sensitivity of the target sequence reached 1.68 copies/μL. On-chip malaria detection proved the feasibility and SNP assay ability of the device. The proposed biosensor with the supporting automatic instruments provides a rapid and quantitative nucleic acid detection method, which is a practical tool for relevant applications.

ASSOCIATED CONTENT

Supporting Information

The Supporting Information is available free of charge at https://pubs.acs.org/doi/10.1021/acssensors.1c01491.

Sequence of synthesized *dhfr* gene and primers, targets and primers for SNP detection, and electrophoresis results of the SNP experiments and turbidity detection results with different template concentrations (PDF)

AUTHOR INFORMATION

Corresponding Authors

Zhi Zheng − *Department of Biochemistry and Molecular Biology, Institute of Basic Medical Sciences, Chinese Academy*

https://doi.org/10.1021/acssensors.1c01491
ACS Sens. 2021, 6, 4057−4066

of Medical Sciences and School of Basic Medicine, Peking Union Medical College, Beijing 100730, China; Email: zhizheng100@126.com

Guoliang Huang − *Department of Biomedical Engineering, School of Medicine, Tsinghua University, Beijing 100084, China; National Engineering Research Center for Beijing Biochip Technology, Beijing 102206, China*; Email: tshgl@mail.tsinghua.edu.cn

Authors

Rongxin Fu − *Department of Biomedical Engineering, School of Medicine, Tsinghua University, Beijing 100084, China*; orcid.org/0000-0002-4547-2269

Wenli Du − *Department of Biomedical Engineering, School of Medicine, Tsinghua University, Beijing 100084, China*

Xiangyu Jin − *Department of Biomedical Engineering, School of Medicine, Tsinghua University, Beijing 100084, China*

Ruliang Wang − *Department of Biomedical Engineering, School of Medicine, Tsinghua University, Beijing 100084, China*

Xue Lin − *Department of Biomedical Engineering, School of Medicine, Tsinghua University, Beijing 100084, China*

Ya Su − *Department of Biomedical Engineering, School of Medicine, Tsinghua University, Beijing 100084, China*; orcid.org/0000-0002-4432-1135

Han Yang − *Department of Biomedical Engineering, School of Medicine, Tsinghua University, Beijing 100084, China*; orcid.org/0000-0002-4475-4803

Xiaohui Shan − *Department of Biomedical Engineering, School of Medicine, Tsinghua University, Beijing 100084, China*

Wenqi Lv − *Department of Biomedical Engineering, School of Medicine, Tsinghua University, Beijing 100084, China*

Complete contact information is available at: https://pubs.acs.org/10.1021/acssensors.1c01491

Author Contributions

R.F., W.D., and X.J. contributed equally. The manuscript was written through contributions of all authors. Conceptualization, R.F. and W.D.; methodology, R.F. and X.J.; performed the experiments, W.D. and X.J.; data analysis, R.F., R.W. and X.L.; wrote and revised the manuscript, R.F., W.D., and X.J.; contributively discussed, reviewed and edited, H.Y., X.S., and W.L.; project administrated, supervised and funding supported, G.H. All authors have read and agreed to the published version of the manuscript. All authors have given approval to the final version of the manuscript.

Funding

This work was supported by National Natural Science Foundation of China (61927819, 81827808, 20170012, 62105177), National Key Research and Development Program of China (2018YFA0704004), Tsinghua University Spring Breeze Fund (20201080510), the Beijing Lab Foundation (20201550018), Tsinghua Autonomous Research Foundation (20194180031, 20201080058) and China Postdoctoral Science Foundation (2020M680591).

Notes

The authors declare no competing financial interest.

■ ACKNOWLEDGMENTS

R.F. acknowledges the Shuimu Tsinghua Scholar Program (2019SM150). All the authors acknowledge Xianbo Luo and Li Ma from Tsinghua University for their help in the system development.

■ REFERENCES

(1) Gootenberg, J. S.; Abudayyeh, O. O.; Lee, J. W.; Essletzbichler, P.; Dy, A. J.; Joung, J.; Verdine, V.; Donghia, N.; Daringer, N. M.; Freije, C. A.; et al. Nucleic acid detection with CRISPR-Cas13a/C2c2. *Science* **2017**, *356*, 438−442.

(2) Ackerman, C. M.; Myhrvold, C.; Thakku, S. G.; Freije, C. A.; Metsky, H. C.; Yang, D. K.; Ye, S. H.; Boehm, C. K.; Kosoko-Thoroddsen, T.-S. F.; Kehe, J.; et al. Massively multiplexed nucleic acid detection with Cas13. *Nature* **2020**, *582*, 277−282.

(3) Wang, M.; Zhang, R.; Li, J. CRISPR/cas systems redefine nucleic acid detection: Principles and methods. *Biosens. Bioelectron.* **2020**, *165*, 112430.

(4) Coronavirus (COVID-19) Dashboards. https://www.arcgis.com/apps/dasboards/bda7594740fd40299423467b48e9ecf6/ (accessed on July 14, 2021).

(5) Esbin, M. N.; Whitney, O. N.; Chong, S.; Maurer, A.; Darzacq, X.; Tjian, R. Overcoming the bottleneck to widespread testing: a rapid review of nucleic acid testing approaches for COVID-19 detection. *RNA* **2020**, *26*, 771−783.

(6) Waller, J. V.; Kaur, P.; Tucker, A.; Lin, K. K.; Diaz, M. J.; Henry, T. S.; Hope, M. Diagnostic Tools for Coronavirus Disease (COVID-19): Comparing CT and RT-PCR Viral Nucleic Acid Testing. *Am. J. Roentgenol.* **2020**, *215*, 834−838.

(7) Lin, C.; Xiang, J.; Yan, M.; Li, H.; Huang, S.; Shen, C. Comparison of throat swabs and sputum specimens for viral nucleic acid detection in 52 cases of novel coronavirus (SARS-Cov-2)-infected pneumonia (COVID-19). *Clin. Chem. Lab. Med.* **2020**, *58*, 1089−1094.

(8) Xiao, A. T.; Tong, Y. X.; Zhang, S. False negative of RT-PCR and prolonged nucleic acid conversion in COVID-19: Rather than recurrence. *J. Med. Virol.* **2020**, *92*, 1755−1756.

(9) Wu, J.; Liu, J.; Li, S.; Peng, Z.; Xiao, Z.; Wang, X.; Yan, R.; Luo, J. Detection and analysis of nucleic acid in various biological samples of COVID-19 patients. *Travel Med. Infect. Dis.* **2020**, *37*, 101673.

(10) Xing, W.; Liu, Y.; Wang, H.; Li, S.; Lin, Y.; Chen, L.; Zhao, Y.; Chao, S.; Huang, X.; Ge, S.; et al. A High-Throughput, Multi-Index Isothermal Amplification Platform for Rapid Detection of 19 Types of Common Respiratory Viruses Including SARS-CoV-2. *Engineering* **2020**, *6*, 1130−1140.

(11) Wang, Y.; Li, K.; Xu, G.; Chen, C.; Song, G.; Dong, Z.; Lin, L.; Wang, Y.; Xu, Z.; Yu, M.; et al. Low-Cost and Scalable Platform with Multiplexed Microwell Array Biochip for Rapid Diagnosis of COVID-19. *Research* **2021**, *2021*, 2813643.

(12) Rhoads, D. D.; Cherian, S. S.; Roman, K.; Stempak, L. M.; Schmotzer, C. L.; Sadri, N. Comparison of Abbott ID Now, DiaSorin Simplexa, and CDC FDA Emergency Use Authorization Methods for the Detection of SARS-CoV-2 from Nasopharyngeal and Nasal Swabs from Individuals Diagnosed with COVID-19. *J. Clin. Microbiol.* **2020**, *58*, e00760−e00820.

(13) Muñoz, H. E.; Riche, C. T.; Kong, J. E.; van Zee, M.; Garner, O. B.; Ozcan, A.; Di Carlo, D. Fractal LAMP: Label-Free Analysis of Fractal Precipitate for Digital Loop-Mediated Isothermal Nucleic Acid Amplification. *ACS Sens.* **2020**, *5*, 385−394.

(14) Hu, Z.; Xu, F.; Sun, G.; Zhang, S.; Zhang, X. Homogeneous multiplexed digital detection of microRNA with ligation-rolling circle amplification. *Chem. Commun.* **2020**, *56*, 5409−5412.

(15) Ereku, L. T.; Mackay, R. E.; Craw, P.; Naveenathayalan, A.; Stead, T.; Branavan, M.; Balachandran, W. RPA using a multiplexed cartridge for low cost point of care diagnostics in the field. *Anal. Biochem.* **2018**, *547*, 84−88.

(16) Pumford, E. A.; Lu, J.; Spaczai, I.; Prasetyo, M. E.; Zheng, E. M.; Zhang, H.; Kamei, D. T. Developments in integrating nucleic acid isothermal amplification and detection systems for point-of-care diagnostics. *Biosens. Bioelectron.* **2020**, *170*, 112674.

(17) Ju, Y.; Kim, H. Y.; Ahn, J. K.; Park, H. G. Ultrasensitive version of nucleic acid sequence-based amplification (NASBA) utilizing a

nicking and extension chain reaction system. *Nanoscale* **2021**, *13*, 10785−10791.
(18) El Wahed, A. A.; Patel, P.; Maier, M.; Pietsch, C.; Rüster, D.; Böhlken-Fascher, S.; Kissenkötter, J.; Behrmann, O.; Frimpong, M.; Diagne, M. M.; et al. Suitcase Lab for Rapid Detection of SARS-CoV-2 Based on Recombinase Polymerase Amplification Assay. *Anal. Chem.* **2021**, *93*, 2627−2634.
(19) Behrmann, O.; Bachmann, I.; Spiegel, M.; Schramm, M.; Abd El Wahed, A.; Dobler, G.; Dame, G.; Hufert, F. T. Rapid Detection of SARS-CoV-2 by Low Volume Real-Time Single Tube Reverse Transcription Recombinase Polymerase Amplification Using an Exo Probe with an Internally Linked Quencher (Exo-IQ). *Clin. Chem.* **2020**, *66*, 1047−1054.
(20) Ivanov, A. V.; Safenkova, I. V.; Zherdev, A. V.; Dzantiev, B. B. Nucleic acid lateral flow assay with recombinase polymerase amplification: Solutions for highly sensitive detection of RNA virus. *Talanta* **2020**, *210*, 120616.
(21) Cao, Y.; Yan, D.; Wu, X. Y.; Chen, Z. Q.; Lai, Y. C.; Lv, L. Q.; Yan, F.; Chen, J. P.; Zheng, H. Y.; Song, X. M. Rapid and visual detection of milk vetch dwarf virus using recombinase polymerase amplification combined with lateral flow strips. *Virol. J.* **2020**, *17*, 102.
(22) Wee, E. J. H.; Lau, H. Y.; Botella, J. R.; Trau, M. Re-purposing bridging flocculation for on-site, rapid, qualitative DNA detection in resource-poor settings. *Chem. Commun.* **2015**, *51*, 5828−5831.
(23) Nair, G.; Ramírez, J. D.; White, A. C., Jr.; Castellanos-Gonzalez, A.; Pinilla, A. E.; Rebolledo, M.; López, M. C.; Richards-Kortum, R. R.; Crannell, Z. Detection of Entamoeba histolytica by Recombinase Polymerase Amplification. *Am. J. Trop. Med. Hyg.* **2015**, *93*, 591−595.
(24) del Río, J. S.; Yehia Adly, N.; Acero-Sánchez, J. L.; Henry, O. Y. F.; O'Sullivan, C. K. Electrochemical detection of Francisella tularensis genomic DNA using solid-phase recombinase polymerase amplification. *Biosens. Bioelectron.* **2014**, *54*, 674−678.
(25) Kober, C.; Niessner, R.; Seidel, M. Quantification of viable and non-viable Legionella spp. by heterogeneous asymmetric recombinase polymerase amplification (haRPA) on a flow-based chemiluminescence microarray. *Biosens. Bioelectron.* **2018**, *100*, 49−55.
(26) Wang, J.; Koo, K. M.; Wee, E. J. H.; Wang, Y.; Trau, M. A nanoplasmonic label-free surface-enhanced Raman scattering strategy for non-invasive cancer genetic subtyping in patient samples. *Nanoscale* **2017**, *9*, 3496−3503.
(27) Cao, Y.; Zheng, K.; Jiang, J.; Wu, J.; Shi, F.; Song, X.; Jiang, Y. A novel method to detect meat adulteration by recombinase polymerase amplification and SYBR green I. *Food Chem.* **2018**, *266*, 73−78.
(28) Wang, X.; Chen, Y.; Chen, X.; Peng, C.; Wang, L.; Xu, X.; Wu, J.; Wei, W.; Xu, J. A highly integrated system with rapid DNA extraction, recombinase polymerase amplification, and lateral flow biosensor for on-site detection of genetically modified crops. *Anal. Chim. Acta* **2020**, *1109*, 158−168.
(29) Shin, Y.; Perera, A. P.; Tang, W. Y.; Fu, D. L.; Liu, Q.; Sheng, J. K.; Gu, Z.; Lee, T. Y.; Barkham, T.; Kyoung Park, M. A rapid amplification/detection assay for analysis of Mycobacterium tuberculosis using an isothermal and silicon bio-photonic sensor complex. *Biosens. Bioelectron.* **2015**, *68*, 390−396.
(30) Banerjee, I.; Aralaguppe, S. G.; Lapins, N.; Zhang, W.; Kazemzadeh, A.; Sönnerborg, A.; Neogi, U.; Russom, A. Microfluidic centrifugation assisted precipitation based DNA quantification. *Lab Chip* **2019**, *19*, 1657−1664.
(31) Andrade, C. M.; Fleckenstein, H.; Thomson-Luque, R.; Doumbo, S.; Lima, N. F.; Anderson, C.; Hibbert, J.; Hopp, C. S.; Tran, T. M.; Li, S.; et al. Increased circulation time of Plasmodium falciparum underlies persistent asymptomatic infection in the dry season. *Nat. Med.* **2020**, *26*, 1929−1940.
(32) Fu, R.; Su, Y.; Wang, R.; Lin, X.; Jiang, K.; Jin, X.; Yang, H.; Ma, L.; Luo, X.; Lu, Y.; et al. Label-free tomography of living cellular nanoarchitecture using hyperspectral self-interference microscopy. *Biomed. Opt. Express* **2019**, *10*, 2757−2767.
(33) Li, Q.; Fu, R.; Zhang, J.; Wang, R.; Ye, J.; Xue, N.; Lin, X.; Su, Y.; Gan, W.; Lu, Y.; et al. Label-Free Method Using a Weighted-Phase Algorithm To Quantitate Nanoscale Interactions between Molecules on DNA Microarrays. *Anal. Chem.* **2017**, *89*, 3501−3507.
(34) Fu, R.; Li, Q.; Wang, R.; Xue, N.; Lin, X.; Su, Y.; Jiang, K.; Jin, X.; Lin, R.; Gan, W.; et al. An interferometric imaging biosensor using weighted spectrum analysis to confirm DNA monolayer films with attogram sensitivity. *Talanta* **2018**, *181*, 224−231.
(35) Mirza, I.; McCloskey, D.; Blau, W. J.; Lunney, J. G. Mechanism of large optical nonlinearity in gold nanoparticle films. *Opt. Lett.* **2018**, *43*, 1455−1458.
(36) Amaral, A. M.; Jorge, K. C.; de Araujo, C. B.; Menezes, L. D. Toward single-shot characterization of nonlinear optical refraction, absorption, and scattering of turbid media. *Phys. Rev. A* **2020**, *102*, 033503.
(37) Park, Y.; Depeursinge, C.; Popescu, G. Quantitative phase imaging in biomedicine. *Nat. Photonics* **2018**, *12*, 578−589.
(38) Fu, R.; Su, Y.; Wang, R.; Lin, X.; Jin, X.; Yang, H.; Du, W.; Shan, X.; Lv, W.; Huang, G. Single cell capture, isolation, and long-term in-situ imaging using quantitative self-interference spectroscopy. *Cytometry, Part A* **2021**, *99*, 601−609.
(39) Xu, Y.; Zheng, Z. Direct RNA detection without nucleic acid purification and PCR: Combining sandwich hybridization with signal amplification based on branched hybridization chain reaction. *Biosens. Bioelectron.* **2016**, *79*, 593−599.
(40) Mockenhaupt, F. P.; Teun Bousema, J.; Eggelte, T. A.; Schreiber, J.; Ehrhardt, S.; Wassilew, N.; Otchwemah, R. N.; Sauerwein, R. W.; Bienzle, U. Plasmodium falciparum dhfr but not dhps mutations associated with sulphadoxine-pyrimethamine treatment failure and gametocyte carriage in northern Ghana. *Trop. Med. Int. Health* **2005**, *10*, 901−908.
(41) Lin, X.; Jin, X.; Xu, B.; Wang, R.; Fu, R.; Su, Y.; Jiang, K.; Yang, H.; Lu, Y.; Guo, Y.; et al. Fast and Parallel Detection of Four Ebola Virus Species on a Microfluidic-Chip-Based Portable Reverse Transcription Loop-Mediated Isothermal Amplification System. *Micromachines* **2019**, *10*, 777.

https://doi.org/10.1021/acssensors.1c01491
ACS Sens. 2021, 6, 4057−4066